Turkish Journal of Electrical Engineering & Computer Sciences

http://journals.tubitak.gov.tr/elektrik/

Research Article

Turk J Elec Eng & Comp Sci
(2018) 26: 2737 – 2752

doi:10.3906/elk-1801-48

A novel FRT strategy based on an analytical approach for PMSG-based wind turbines with ESS power rating reduction

Farid ATASH BAHAR[1], **Ali AJAMI**[1,*], **Hossein MOKHTARI**[2], **Hossein HOJABRI**[3]
[1]Department of Electrical Engineering, Azarbaijan Shahid Madani University, Tabriz, Iran
[2]Department of Electrical Engineering, Sharif University of Technology, Tehran, Iran
[3]Department of Electrical Engineering, Shahid Bahonar University, Kerman, Iran

Received: 05.01.2018 • **Accepted/Published Online:** 03.04.2018 • **Final Version:** 28.09.2018

Abstract: In this paper an analytical approach is proposed to formulate the proper set of phase currents reference to ride the permanent magnet synchronous generator (PMSG)-based wind turbine (WT) through faults properly, regardless of fault type. Hence, the WT is forced to inject required reactive current by grid codes together with active power injection, to help support grid frequency during faults and reduce the energy storage system (ESS) power rating. Moreover, it prevents pulsating active power injection to the grid. During grid faults, the DC-link voltage is controlled by the ESS instead of the grid-side converter (GSC) and the GSC controller applies calculated reference currents. The ESS helps DC-link voltage oscillations to be significantly suppressed during the fault. MPCC is applied to handle fast transient states. The main contributions of this paper are first presenting an analytical approach to calculate a proper set of unbalanced reference currents to ride the PMSG-based WT through faults, disregarding grid fault type, while considering phase current protection threshold and second ESS power rating reduction. Different simulations have been carried out to verify the validity of the proposed approach and the efficiency of the whole control system.

Key words: Permanent magnet synchronous generator, asymmetric fault, unbalanced voltages, unbalanced currents, fault ride through, energy storage system, DC-link voltage

1. Introduction

Among all other renewable energy sources, wind energy has been growing very rapidly in recent years [1]. Wind energy conversion systems (WECSs) are commonly based on variable speed wind turbines (WTs) consisting of doubly fed induction generators (DFIGs) [2–4] and permanent magnet synchronous generators (PMSGs) [5]. DFIG-based WECSs present some drawbacks like less reliability and high maintenance cost according to applying gearbox and slip rings [6,7]. Aside from these, PMSG-based WECSs attracted more attention thanks to their inherent merits like less maintenance cost and more reliability, because of gearbox removal, wide operation speed range and better power factor, despite their initial installation cost and greater converter loss [8,9]. Furthermore, PMSG-based WECSs can easily withstand grid disturbances and contribute more to grid stability [10].

As the importance of the wind power generation rose, utility grid operators started to require them to behave in a closer manner to conventional power plants [11] and created some regulations, which are called grid codes [12], in which the capability to ride through grid faults and voltage disturbances is demanded. These

*Correspondence: ajami@azaruniv.edu

regulations have two major requirements in common. First, they want the WECSs to stay connected to the grid in abnormal grid conditions [11,12]. WECSs just can be disconnected when the voltage profile goes under the grid code's guideline as shown in Figure 1a [12]. Second, WECSs should provide an ancillary service to the grid during grid disturbances by injecting a predefined amount of reactive current [11–14]. Figure 1b shows the expected reactive current to be injected by the WECS, according to voltage drop level for the German grid code [12].

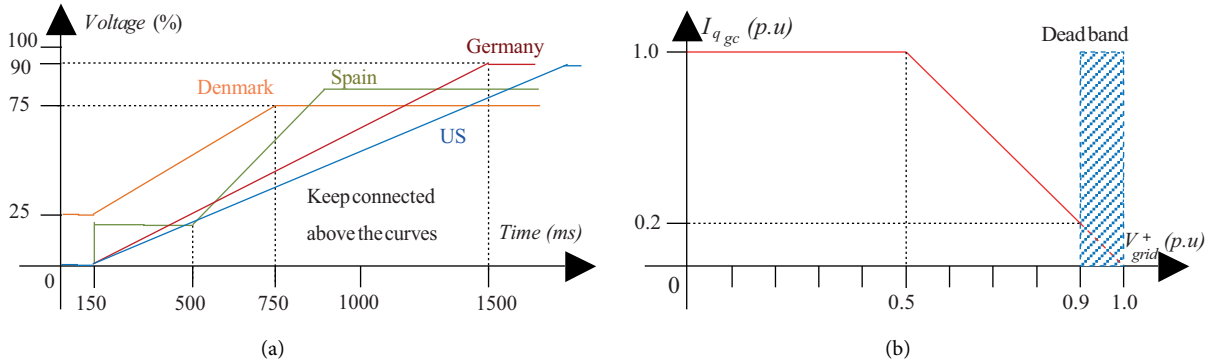

Figure 1. (a) Grid code guidelines for WT disconnection during faults [13]; (b) Required reactive current considering the voltage sag profile in the German grid code [12].

During grid faults, interaction between the arisen negative sequence voltage and injected currents leads to the presence of double-grid-frequency oscillations in the injected active power and DC-link voltage, which is not desired [8,15]. Against the fact that asymmetric faults are from the absolute majority [16], most of the grid codes are set to aim for only positive sequence current. When WECSs inject pure positive sequence reactive current, not only is positive sequence voltage boosted but also negative and zero sequence voltages are boosted too, because of the coupling nature of different sequence networks. This may lead to overvoltage in one or two nonfaulty phases [14,17]. In order to make the unbalanced grid voltages more balanced, negative sequence current injection alongside positive sequence current is vital [14]. In addition, it is possible to eliminate the active power or DC-link voltage oscillatory term by injecting a proper set of unbalanced currents in accordance with the voltage dipping profile [18,19].

Because of GSC reaching its current protection limit, there will be a power mismatch between the turbine's generated and injected active power during voltage sags that causes excessive power burden in the DC-link and DC overvoltage [20–22] that should be overcome. Utilizing turbine inertia as energy storage causes mechanical tensions as it is working near nominal speed [23] and in deep voltage sags the capacity of turbine inertia is not sufficient to absorb extra power. Hence, additional protection devices such as a braking chopper (BC) [20,22,23] and ESS [23–26] are utilized to assist the WECS operation during voltage sags.

The fault ride-through (FRT) strategy is about how a WECS contributes to the faulty grid or what current components WECS is injecting to the grid [27,28]. Some of the released strategies are not on an analytical basis [8,13,19] and the formulations in [8,9,29] are complicated and implicit. In some others, grid code requirements (GCRs) are not taken into account completely and current references are defined according to predefined power references [8,18,29–33], missing the fact that in grid codes just current values are mentioned, not power values. In some of the strategies like [8,13,23,30,33] the injected currents are balanced. This not only neglects the benefits of unbalanced current injection but also pulsating active power is injected into the grid, in the case

of asymmetrical faults. The methodology in [23] does not support grid frequency as injected active power is zero during the fault. DC-link voltage control is very important in the FRT strategy but is not mentioned in [13,30–32]. Moreover, in [8,21] DC-link voltage control is maintained by a machine-side converter (MSC), which leads to more mechanical stresses. In [8] the generated active power is limited to avoid the overcurrent (OC) problem in the GSC. Another important aspect is to maintain the amplitude of phase currents in an acceptable margin, which is missed in some cases [21,31,32]. In [18] reference currents are scaled to the nominal current capacity of the GSC, which may result in disagreement with the values mentioned in the grid code.

In the present paper an analytical approach is proposed, in which unbalanced current references for the GSC are calculated explicitly by clear formulation, which completely complies with GCRs and is in accordance with the voltage dipping profile and severity, without knowing about fault type. The oscillating active power flow is prevented and DC-link voltage control is transferred from GSC to ESS during the fault. The GSC injects the required amount of reactive current and an active current component, in order to reduce ESS power rating, without OC occurrence. Furthermore, ESS operation majorly reduces DC-link voltage fluctuation. Considering the fact that lower and constant switching frequency is very prominent at MW level and according to rapid nature of transient states MPCC is applied as a satisfactory alternative, which is proposed in [34] and applied in [30,35].

The present paper is organized as follows. Section 2 is dedicated to formulate phase current limitation and reference current calculation. Section 3 contains a description of the coordinated controller for the GSC, ESS, and BC. Numerical examples and simulation results are presented in section 4 in order to validate the obtained equations and to show the effective performance of the proposed strategy under different faulty conditions. Finally, a brief conclusion is presented in section 5.

2. The proposed strategy

A typical PMSG-based WECS consists of three main pieces of equipment: a WT, a PMSG, and a back-to-back (BTB) converter. The MSC attains variable speed operation to extract the maximum possible wind energy and the GSC delivers the synchronized power to the grid. The configuration of a PMSG-based WT accompanied by a BC and an ESS is depicted in Figure 2.

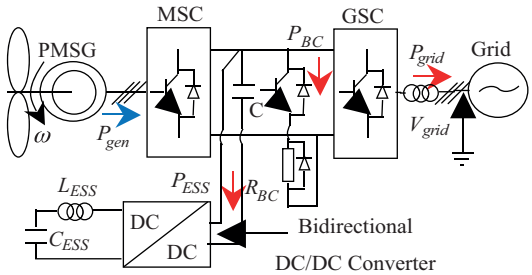

Figure 2. PMSG-based WT configuration with ESS and BC.

Grid codes want the WECS to stay connected to the grid during the fault time interval and inject a special amount of reactive current with respect to the positive voltage drop level. For example the German grid code requires reactive current injection by the WT to support grid voltage as follows:

$$\begin{cases} I_{q_{gc}} = 1p.u. & V^{+}_{grid} < 0.5p.u. \\ I_{q_{gc}} = -2V^{+}_{grid} + 2 & 0.5p.u. \leq V^{+}_{grid} < 0.9p.u. \end{cases} \quad (1)$$

The apparent power (S) in unbalanced condition can be expressed in terms of positive and negative voltage and current sequences as

$$S = VI* = (e^{j\omega t} \times V_{dq}^{+} + e^{-j\omega t} \times V_{dq}^{-})(e^{j\omega t} \times I_{dq}^{+} + e^{-j\omega t} \times I_{dq}^{-})^{*} = P + jQ \tag{2}$$

Here 'd' and 'q' subscripts stand for direct and quadrature components. The d-q decomposition is very suitable for power description in unbalanced circumstances, because it deals with DC values and helps to identify power elements clearly. The above multiplication can be rewritten in matrix form, which leads to active and reactive power components definition just like

$$\begin{bmatrix} \overline{P} \\ P_{c2} \\ P_{s2} \\ \overline{Q} \\ Q_{c2} \\ Q_{s2} \end{bmatrix} = \frac{3}{2} \begin{bmatrix} V_d^{+} & V_q^{+} & V_d^{-} & V_q^{-} \\ V_d^{-} & V_q^{-} & V_d^{+} & V_q^{+} \\ V_q^{-} & -V_d^{-} & -V_q^{+} & V_d^{+} \\ V_q^{+} & -V_d^{+} & V_q^{-} & -V_d^{-} \\ V_q^{-} & -V_d^{-} & V_q^{+} & -V_d^{+} \\ -V_d^{-} & -V_q^{-} & V_d^{+} & V_q^{+} \end{bmatrix} \begin{bmatrix} I_d^{+} \\ I_q^{+} \\ I_d^{-} \\ I_q^{-} \end{bmatrix} \tag{3}$$

Here

$$\begin{cases} P(t) = \overline{P} + P_{c2}\cos(2\omega t) + P_{s2}\sin(2\omega t) \\ Q(t) = \overline{Q} + Q_{c2}\cos(2\omega t) + Q_{s2}\sin(2\omega t) \end{cases} \tag{4}$$

First, it is assumed that I^{+} and I^{-} are positive and negative sequence components of the currents supposed to be injected to the grid, which are attached to their respective synchronous reference frames, rotating with ω angular frequency clockwise and counterclockwise with initial phase angles of φ^{+} and φ^{-}, respectively. The rotating space vector of I^{+} and I^{-} related to the stationary $\alpha\beta$ reference frame is illustrated in Figure 3a.

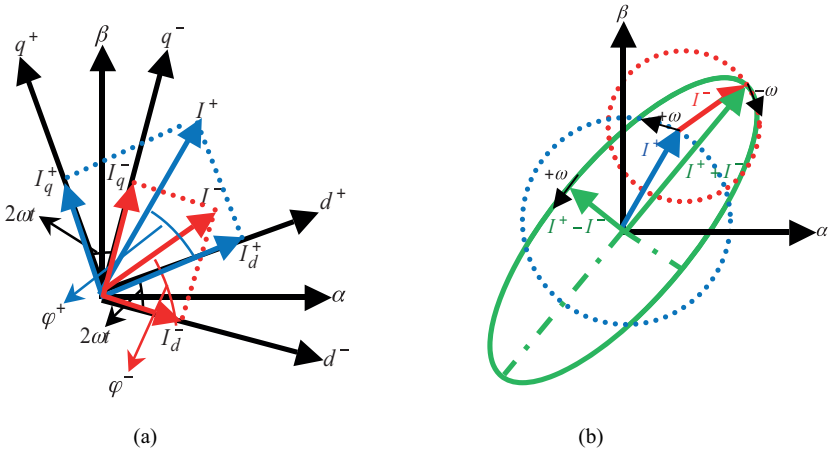

Figure 3. (a) Positive and negative sequence currents projection on their relevant synchronous frame toward stationary $\alpha\beta$ frame; (b) Resultant current space vector.

First both d-q components of I^{-} should be projected on both positive sequence d-q axes, to be added to d-q components of I^{+}. Doing so yields d-q components of the resultant current space vector on the positive sequence reference frame, like Figure 3b. After time passing as much as t seconds, the angular difference between

the d axis (or q axis) of the positive and negative sequences reference frames, is 2ωt. The resultant current space vector on positive sequence reference frame can be formed as

$$\begin{cases} I_{d+} = I_d^+ + I_d^- \cos(2\omega t) + I_q^- \sin(2\omega t) \\ I_{q+} = I_q^+ - I_d^- \sin(2\omega t) + I_q^- \cos(2\omega t) \end{cases} \tag{5}$$

Here subscripts '$d+$' and '$q+$' refer to d and q components of the resultant space vector on the positive sequence reference frame. The amplitude of the resultant current space vector ($|I_+|$) is obtained by

$$\begin{aligned} |I_+|^2 =& I_{d+}^2 + I_{q+}^2 = I_d^{+2} + I_q^{+2} + I_d^{-2} + I_q^{-2} \\ &+ 2I_d^+ I_d^- \cos(2\omega t) + 2I_d^+ I_q^- \sin(2\omega t) \\ &- 2I_q^+ I_d^- \sin(2\omega t) + 2I_q^+ I_q^- \cos(2\omega t) \\ =& I_d^{+2} + I_q^{+2} + I_d^{-2} + I_q^{-2} + 2(I_d^+ I_d^- + I_q^+ I_q^-)\cos(2\omega t) + 2(I_d^+ I_q^- - 2I_q^+ I_d^-)\sin(2\omega t) \end{aligned} \tag{6}$$

The summation of a "sin" term and a "cos" term can turn into just one new "cos" term, according to the fallowing trigonometric rule:

$$A\cos(\alpha) + B\sin(\alpha) = \sqrt{A^2 + B^2}\cos(\alpha - \tan^{-1}\frac{B}{A}) \tag{7}$$

Applying the abovementioned rule gives

$$\begin{aligned} |I_+|^2 =& I_d^{+2} + I_q^{+2} + I_d^{-2} + I_q^{-2} \\ [1.2em] &+ 2\sqrt{(I_d^+ I_d^- + I_q^+ I_q^-)^2 + (I_d^+ I_q^- - 2I_q^+ I_d^-)^2}\cos(2\omega t - \tan^{-1}\frac{I_d^+ I_q^- - 2I_q^+ I_d^-}{I_d^+ I_d^- + I_q^+ I_q^-}) \end{aligned} \tag{8}$$

As the maximum and minimum values of the "cos" function are '+1' and '–1', respectively, the maximum of the term $|I_+|^2$ would be

$$|I_+|^2_{\max} = I_d^{+2} + I_q^{+2} + I_d^{-2} + I_q^{-2} + 2\sqrt{(I_d^+ I_d^- + I_q^+ I_q^-)^2 + (I_d^+ I_q^- - 2I_q^+ I_d^-)^2} \tag{9}$$

Locking positive and negative sequence reference frames to positive and negative sequence voltage vectors ($V_q^+ = V_q^- = 0$) turns the power definition into

$$\begin{bmatrix} \overline{P} \\ P_{c2} \\ P_{s2} \\ \overline{Q} \\ Q_{c2} \\ Q_{s2} \end{bmatrix} = \frac{3}{2} \begin{bmatrix} V_d^+ & 0 & V_d^- & 0 \\ V_d^- & 0 & V_d^+ & 0 \\ 0 & -V_d^- & 0 & V_d^+ \\ 0 & -V_d^+ & 0 & -V_d^- \\ 0 & -V_d^- & 0 & -V_d^+ \\ -V_d^- & 0 & V_d^+ & 0 \end{bmatrix} \begin{bmatrix} I_d^+ \\ I_q^+ \\ I_d^- \\ I_q^- \end{bmatrix} \tag{10}$$

Considering the abovementioned equation and evaluating P_{c2} and P_{s2} equal to zero will lead to

$$\begin{aligned} P_{c2} = \tfrac{3}{2}(V_d^- I_d^+ + V_d^+ I_d^-) = 0 \Rightarrow I_d^- = -\tfrac{V_d^-}{V_d^+} I_d^+ \\ P_{s2} = \tfrac{3}{2}(-V_d^- I_q^+ + V_d^+ I_q^-) = 0 \Rightarrow I_q^- = \tfrac{V_d^-}{V_d^+} I_q^+ \end{aligned} \tag{11}$$

$$\begin{aligned} P_{c2} &= \tfrac{3}{2}(V_d^- I_d^+ + V_d^+ I_d^-) = 0 \Rightarrow I_d^- = -\tfrac{V_d^-}{V_d^+} I_d^+ \\ P_{s2} &= \tfrac{3}{2}(-V_d^- I_q^+ + V_d^+ I_q^-) = 0 \Rightarrow I_q^- = \tfrac{V_d^-}{V_d^+} I_q^+ \end{aligned} \tag{12}$$

Combining Eqs. (9), (11), and (12) results in

$$\begin{aligned} |I_+|^2_{\max} =& (1 + (\frac{-V_d^-}{V_d^+})^2) I_d^{+2} + (1 + (\frac{V_d^-}{V_d^+})^2) I_q^{+2} + 2(\frac{V_d^-}{V_d^+})(I_d^{+2} + I_q^{+2}) \\ =& (1 + \frac{V_d^-}{V_d^+})^2 (I_d^{+2} + I_q^{+2}) \end{aligned} \tag{13}$$

The resultant current amplitude should be smaller than the GSC rated current, which means $|I_+|_{\max} < I_{rated}$ or $|I_+|^2_{\max} < I^2_{rated}$. Then it can be concluded that

$$I_d^{+2} \leq \frac{I^2_{rated}}{(1 + \frac{V_d^-}{V_d^+})^2} - I_q^{+2} \Rightarrow I_d^+ \leq \sqrt{\frac{I^2_{rated}}{(1 + \frac{V_d^-}{V_d^+})^2} - I_q^{+2}} \tag{14}$$

Then the maximum value for I_d^+ will be

$$I_{d\max}^+ = \sqrt{\frac{I^2_{rated}}{(1 + \frac{V_d^-}{V_d^+})^2} - I_q^{+2}} \tag{15}$$

The I_q^+ and I_q^- values are defined according to (12) together with required reactive current in the grid code (Eq. (1)), which leads to a system of linear equations as below:

$$\begin{cases} I_q^- = \frac{V_d^-}{V_d^+} I_q^+ \\ I_q^+ + I_q^- = I_{q_{gc}} \end{cases} \tag{16}$$

Here $I_{q_{gc}}$ is required reactive current in the grid code.

The cost of establishing a high power ESS is too high; thus it is preferred to choose the ESS power rating as 0.3 of the WT rated power [23,26]. As in most grid faults injecting the reactive current required by the grid code does not occupy the whole current capacity of the GSC, injecting a portion of the generated active power during the fault can help reduce the ESS power rating, while maintaining the ESS's healthy operation. In fact, in the proposed FRT strategy, by injecting a portion of the generated active power, a considerable part of the generated power by the WT is handled, which can help reducing the ESS size and power rating, because the amount of nondeliverable power, mismatched between the WT and the faulty grid, is reduced. Thus, the amount of power that should be treated by the ESS (and BC) is equal to the subtraction of the injected power from the generated power, and hence the power to be treated is reduced. This allows us to reduce the power rating of the ESS, where the ESS power rating is chosen as 0.1 p.u. In order to reduce the ESS power rating from 0.3 p.u. to 0.1 p.u., in this strategy 0.2 p.u. of average active power is injected into the grid during the fault (if possible) and the rest is absorbed by the ESS or dissipated by the BC. The I_d^+ value will be chosen in

a way that the resultant average active power equals to 0.2 p.u., but if such I_d^+ exceeds $I_{d\max}^+$ value, which is defined in (15), then $I_{d\max}^+$ will be chosen as I_d^+ value.

Considering first row of Eq. (10) (average active power relation) and (11) we have

$$\begin{cases} P_{grid} = 0.2P_{rated} = \frac{3}{2}(V_d^+ I_d^+ + V_d^- I_d^-) \\ I_d^- = -\frac{V_d^-}{V_d^+} I_d^+ \end{cases} \Rightarrow I_d^+ = \frac{0.4P_{rated}V_d^+}{3(V_d^{+2} - V_d^{-2})} \tag{17}$$

Now I_d^+ and I_d^- are selected as below:

$$\begin{cases} if \frac{0.4P_{rated}V_d^+}{3(V_d^{+2}-V_d^{-2})} \le I_{d\max}^+ \Rightarrow I_d^+ = \frac{0.4P_{rated}V_d^+}{3(V_d^{+2}-V_d^{-2})} \\ if \frac{0.4P_{rated}V_d^+}{3(V_d^{+2}-V_d^{-2})} > I_{d\max}^+ \Rightarrow I_d^+ = I_{d\max}^+ \end{cases} \quad and \quad I_d^- = -\frac{V_d^-}{V_d^+} I_d^+ \tag{18}$$

In fact, by injecting a portion of active power (0.2 p.u.), a part of the WT's generated power is handled, which can help reducing the ESS size and power rating, because the amount of nondeliverable power is reduced and a smaller ESS with less power rating can handle the excess power in collaboration with the BC. This idea is one of the contributions in the proposed method.

Now all the four current elements of the injected current by the GSC of the WECS (I_d^+, I_q^+, I_d^-, and I_q^-) are defined clearly, providing the required reactive current in GCRs without injecting pulsating active power. Moreover, the power rating of the ESS is reduced from 0.3 p.u. to 0.1 p.u., which is very important and significantly reduces the high cost of ESS establishment.

3. Description of the coordinated controller for the GSC, ESS, and BC

In normal conditions, the GSC injects just I_d^+ (no reactive current) in a way that injected power equals generated power and maintains DC-link voltage at its reference value by controlling I_d^+. However, in a faulty grid condition, the GSC gives up controlling DC-link voltage to the ESS and generates currents according to reference signals obtained in the previous section itself. The GSC controller configuration can be seen in Figure 4. In a faulty grid condition, I_d^+, I_d^-, I_q^+, and I_q^- are generated according to (16) and (18). Then the current components are fed to the related (positive or negative sequence) inverse Park transformation block, which gives out positive and negative sequence "abc" currents, separately. The reference angle for transformation is extracted by two separate phase-locked loops (PLLs), each dedicated to one of the sequences. In addition, grid voltages are decomposed into d-q components through a dual-double synchronous reference frame (DDSRF). As the positive and negative sequence voltages are generated by using their own reference angle, the "q" component of both sequence voltages will be zero. After that, these "abc" currents are added together to give out final current reference signals in "abc" form, which is fed to the MPCC block and the GSC will synthesize the currents.

MPCC is exerted in order to modulate reference currents for both GSC and MSC, which is discussed here briefly. Model predictive control (MPC) is based on the fact that just a limited number of feasible switching configurations can be generated by a converter and variables can be predicted for each state, based on the model. A cost function (CF) is evaluated for predicted variables that are to be controlled. The future value of

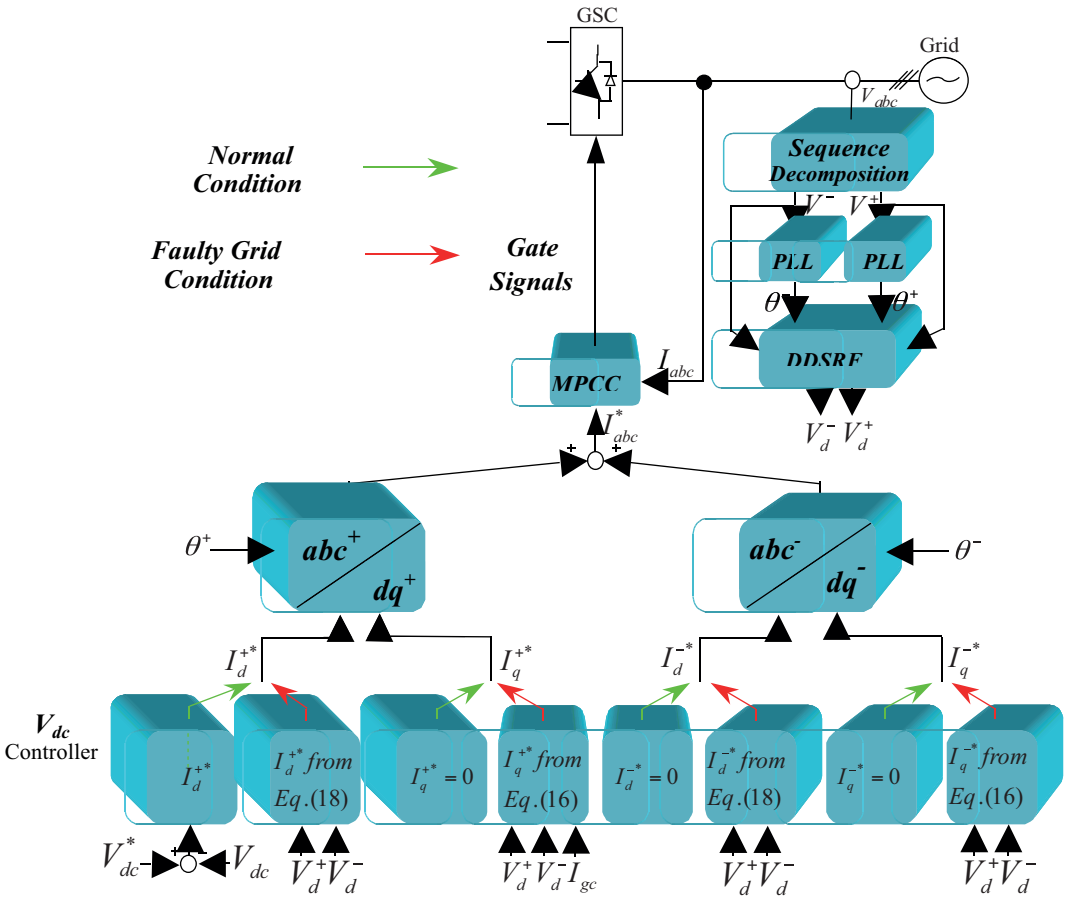

Figure 4. GSC controller block diagram (for both normal and FRT operation).

the variable is compared with the measured value and a cost function-minimizing configuration is chosen [34]. The CF to control the output current of the converter, assuming negligible change of reference values in one sampling period, is expressed in $\alpha\beta$ coordinates as

$$CF = |I^*_\alpha(n) - I^p_\alpha(n+1)| + \left|I^*_\beta(n) - I^p_\beta(n+1)\right| \tag{19}$$

Here '*' and 'p' superscripts stand for reference and predicted values, respectively.

The dynamic equation of load (here the grid) can be described as

$$v = Ri + L\frac{di}{dt} + e \tag{20}$$

In the abovementioned equation, "v" is inverter output voltage vector, "i" is load current vector (here injected current to the grid), "e" is load's back-EMF (here grid voltage), and R and L are load resistance and inductance (here equivalent resistance and inductance of the output filter and grid impedance).

A discrete-time model is used to predict load current in next sampling interval from voltages and measured currents at the "n'th" sampling instant. The forward Euler method is used to approximate load current

derivative as

$$\frac{di}{dt} = \frac{i(n+1) - i(n)}{T_s} \tag{21}$$

Substituting (21) in (20) leads to prediction of load current at 'n+1' interval for seven possible output voltage vectors, v(n), (related to different possible switching configurations), by

$$i^p(n+1) = (1 - \frac{RT_s}{L})i(n) + \frac{T_s}{L}(v(n) - \hat{e}(n)) \tag{22}$$

Here $\hat{e}(n)$ is estimated grid voltage that can be calculated from (20) and measured voltages and currents, considering high sampling frequency (e.g., $\hat{e}(n) = \hat{e}(n-1)$) as

$$\hat{e}(n) = v(n-1) - \frac{L}{T_s}i(n) - (R - \frac{L}{T_s})i(n-1) \tag{23}$$

Now it is possible to predict $i^p(n+1)$ for all possible inverter switching configurations and the one that minimizes the CF will be applied in the next sampling instant.

The ESS has two control loops. The outer loop stabilizes DC-link voltage and generates the reference value for the inner current loop, which controls the electric double-layer capacitor (EDLC)'s current. The outer loop forces the ESS to absorb as much of the power that stabilized DC-link voltage at its reference. ESS power is calculated from EDLC current and voltage (I_{ESS} and V_{ESS}) as

$$P_{ESS} = V_{ESS}.I_{ESS} \tag{24}$$

In order to control the EDLC's current, the DC/DC converter's boost inductance voltage (V_L) should be inspected:

$$V_L = L_{ESS}\frac{dI_{ESS}}{dt} = D_{ESS}V_{DC} - V_{ESS} \tag{25}$$

Here L_{ESS} and D_{ESS} are the boost inductance and duty cycle of the bidirectional DC/DC converter, which can be described as

$$D_{ESS} = \frac{V_{ESS} + V_L^*}{V_{DC}} \tag{26}$$

In a faulty grid condition, when the ESS capacity is not sufficient to absorb the whole extra power, the BC is activated to treat residue surplus power:

$$P_{BC} = P_{gen} - P_{grid} - P_{ESS} \tag{27}$$

The S_3 switch duty cycle of the BC in Figure 5 is calculated as

$$D_{BC} = \frac{R_{BC}}{V_{DC}^2}P_{BC} \tag{28}$$

The control gains can be found in the Table.

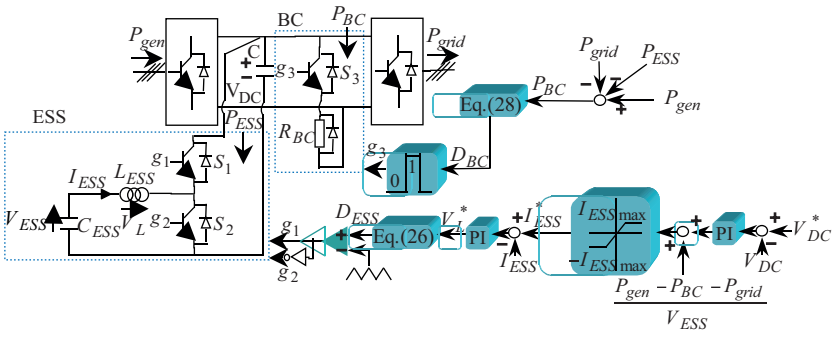

Figure 5. ESS and BC controllers block diagram.

Table. System characteristics.

Wind Turbine		PMSG	
Rated power	3 MW	Rated Power	2.96 MW
Base Wind Speed	12 m/s	Stator Voltage/Frequency	3 kV/9.75 Hz
Blade Radios	43.35 m	Stator Resistance	37.521 mΩ
Air Density	1.225 kg/m^3	Stator Inductance	9.75 mH
Max. Power Conversion Coefficient	0.45	Number of Pole Pairs	26
Optimal Tip Speed Ratio	8.5128	Moment of Inertia	6327
Utility Grid			
Voltage/Frequency		20 kV/60 Hz	
X/R Ratio (R+jX)		12 (0.192+j0.016 Ω)	
Medium Transformer Configuration		Y/Δ	
Medium Transformer Voltage Conversion Ratio		3 kV/20 kV	
Medium Transformer Short Circuit Impedances		Prim. Winding (3 kV): 0.001+j0.001 Ω Sec. winding (20 kV): 0.0067+j0.0067 Ω	
Back-to-Back Converter		ESS and BC	
DC-link Capacitance	5 mF	ESS Power Rating	300 kW
DC-link Voltage	5 kV	Capacitance of EDLC	10 F
Switching Frequency	5 kHz	ESS Operating Voltage	2500 V
Grid-Side Filter Resistance	1 mΩ	BC Resistance	10 Ω
Grid-Side Filter Inductance	10 mH	ESS and BC Switching Frequency	5 kHz
V_{DC} Controller (Normal Condition)	$K_p = -10$ $K_I = -20$	ESS's V_{DC} Controller (Fault Condition) ESS's Current Controller (Fault Condition)	$K_p = 0.6$ $K_I = 18$ $K_p = 300$ $K_I = 300$

4. Operation analysis and simulation results

To verify the effectiveness of the proposed FRT strategy, three different simulation scenarios for FRT of a 3 MW PMSG-based WECS, including two asymmetric faults and one symmetric fault, were performed and the results are discussed. In all cases the fault occurs in 0.6 to 1 s interval and the fault impedance is 0.001 + j0.0019. The simulations are implemented in MATLAB/SIMULINK environment with a solution time step of 1 μs. The system characteristics can be found in the Table.

4.1. First scenario: φ-g fault at the PCC

In this scenario a single phase-to-ground fault (phase "b") takes place at the point of common coupling (PCC), causing an asymmetric voltage drop at the WT connection bus as follows: V_a = 1588 V, V_b = 1469 V, and V_c = 2449 V (V_d^+ = 1752 V, V_d^- = 692 V, and $V_q^+ = V_q^- = 0$). According to the German grid code, 0.57 p.u. reactive current should be injected into the grid. Applying Eq. (16) gives I_q^+ = 333 A and I_q^- = 132 A. Calculated I_d^+ and $I_{d\max}^+$ are 270.5 A and 481.5 A, respectively. As I_d^+ does not exceed $I_{d\max}^+$, then I_d^+ will be chosen as 270.5 A. Consequently I_d^- equals –107 A. In this way 600 kW (0.2 p.u.) active power (out of 2.12 MW generated power) will be delivered to the grid. As the extra power (1.52 MW) exceeds the power absorbed by the ESS (300 kW), 1.22 MW will be dissipated by the BC. The ESS maintains the DC-link voltage at its reference value (5 kV) properly and reduces voltage oscillations significantly. Figure 6 (simulation results for this case) shows good performance of the controllers, ESS, BC, and overall system together with the chosen strategy. As can be seen, the generated active power is fully handled during the fault without overvoltage

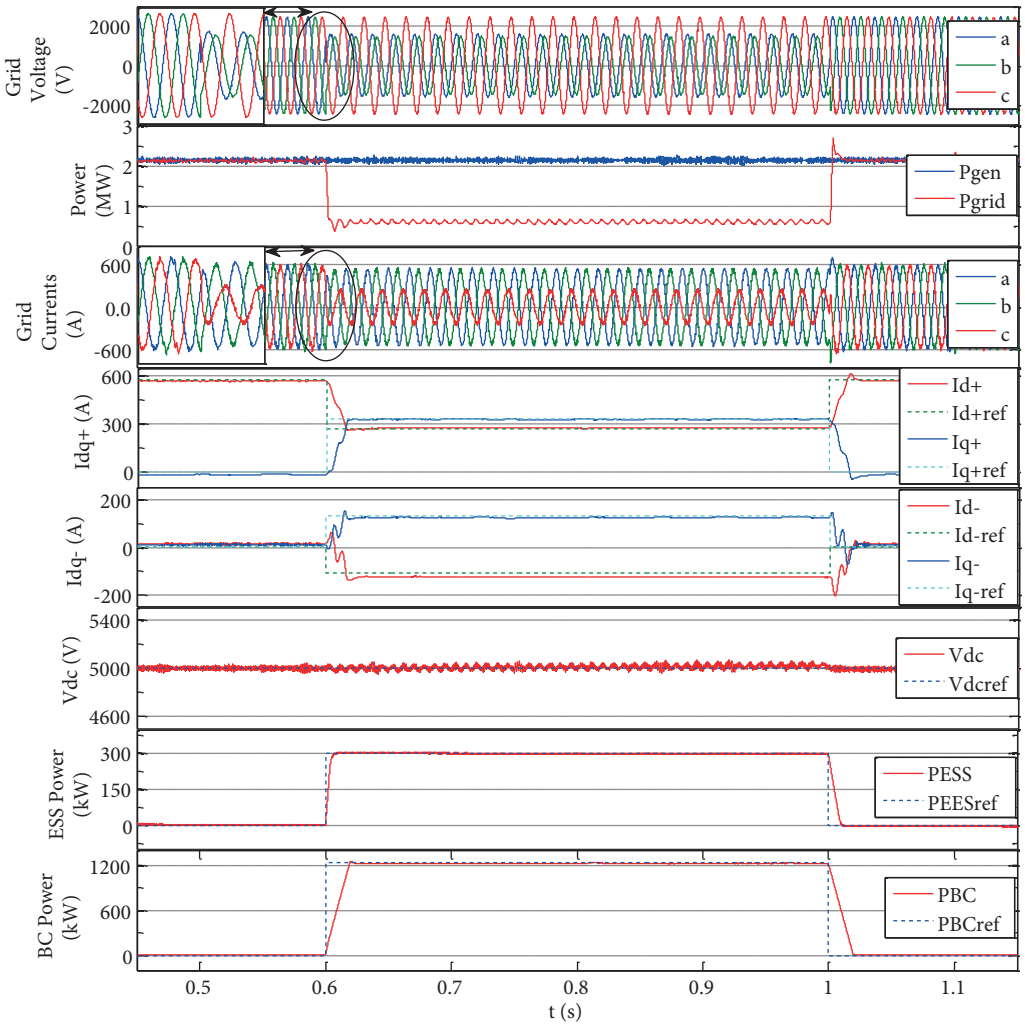

Figure 6. Simulation results for the first scenario, from top to bottom: grid voltages, generator power and injected power to the grid, grid currents, positive sequence dq components of grid current, negative sequence dq components of grid current, DC-link voltage, ESS power, and BC power.

occurrence in the DC-link, despite ESS capacitance reduction. Furthermore, current components follow their reference value accurately, without OC in any phase.

4.2. Second scenario: 2 φ-g fault at the PCC

A two phase-to-ground fault (phases "a" and "b") at the PCC will turn the WT connection bus voltages asymmetric as follows: V_a = 904 V, V_b = 1640 V, and V_c = 1824 V (V_d^+ = 1406 V, V_d^- = 532 V, and $V_q^+ = V_q^- = 0$). The required reactive current would be 0.85 p.u., according to GCRs. In this case, calculated I_d^+ (332 A) is greater than $I_{d\max}^+$ (310 A). Then I_d^+ will be chosen equal to $I_{d\max}^+$. The other current components are calculated as I_d^- = –117 A, I_q^+ = 505 A, and I_q^- = 191 A. In this way, 560 kW power is injected into the grid, 300 kW is stored in the ESS, and the rest (1.26 MW) is mitigated by the BC. Hence, DC-link voltage is maintained around 5 kV, accurately without considerable fluctuations. Simulation results for this scenario are shown in Figure 7. As is shown, the mismatched active power is shouldered by the reduced size ESS and BC during the fault accurately, without DC overvoltage. In addition, current components satisfy the GCRs without

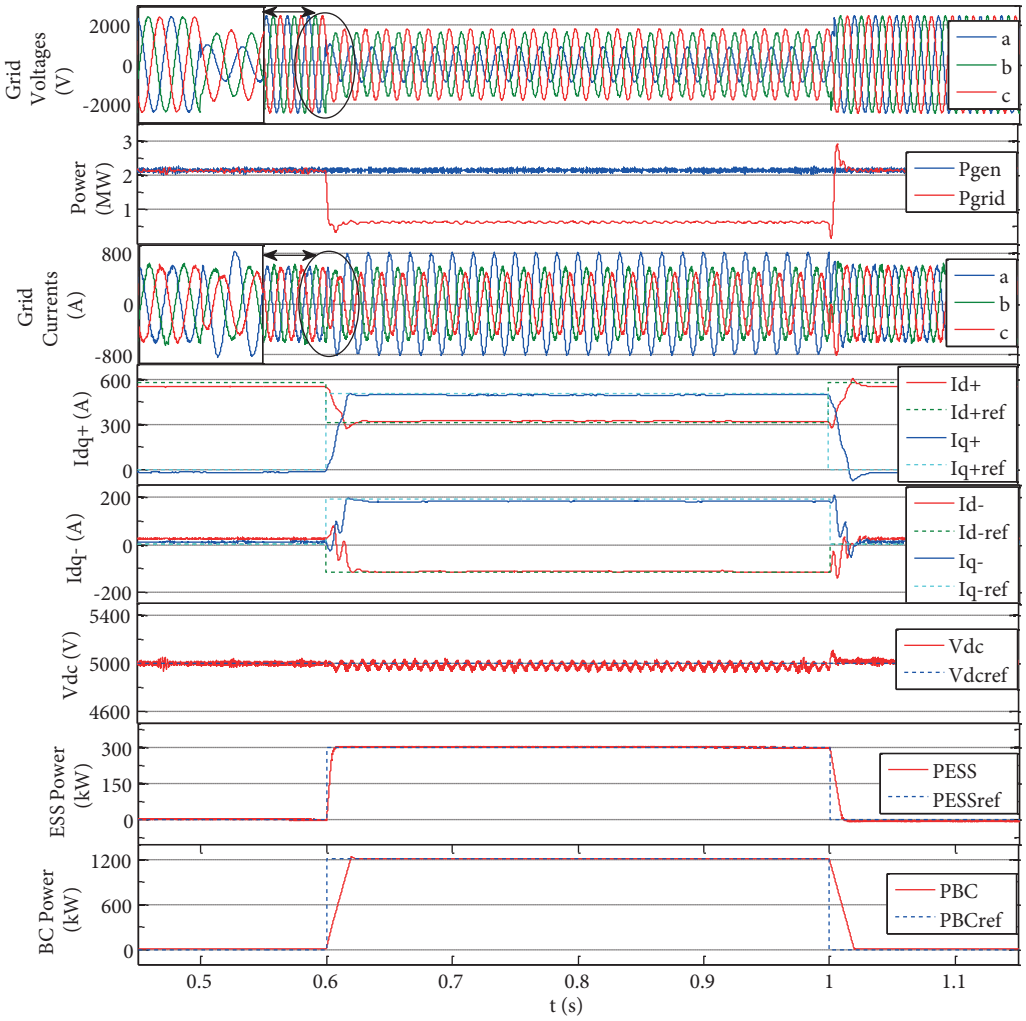

Figure 7. Simulation results for second scenario, from top to bottom: grid voltages, generator power and injected power to the grid, grid currents, positive sequence dq components of grid current, negative sequence dq components of grid current, DC-link voltage, ESS power, and BC power.

current threshold violation. It can be seen that phase "a" current has reached its nominal value, as I_d^+ has reached $I_{d\max}^+$ limitation.

4.3. Third scenario: 3 φ-g fault at the PCC

As this kind of fault (three phase-to-ground) is classified as symmetric, Bus 2 voltage will drop to 976 V, equally, for all phases ($V_d^+ = 976$ V, $V_d^- = V_q^+ = V_q^- = 0$). Considering Eqs. (16) and (18) impels the negative sequence current component to become zero and as the PCC voltage drops to a value less than 0.5 p.u., the WECS should inject 1 p.u. pure reactive current into the grid (Eq. (1)), which means $I_q^+ = 816.6$ A and $I_d^+ = I_d^- = I_q^- = 0$. Consequently no active power is delivered to the grid, 300 kW of the generated power flows into the ESS, and the rest (1.82 MW) is dissipated by the BC, which makes the DC-link voltage to stay at 5 kV precisely, without significant oscillations.

Simulation results for this scenario are depicted in Figure 8. As is shown, currents are balanced and the required reactive current is injected without active power injection and the extra active power is coped with

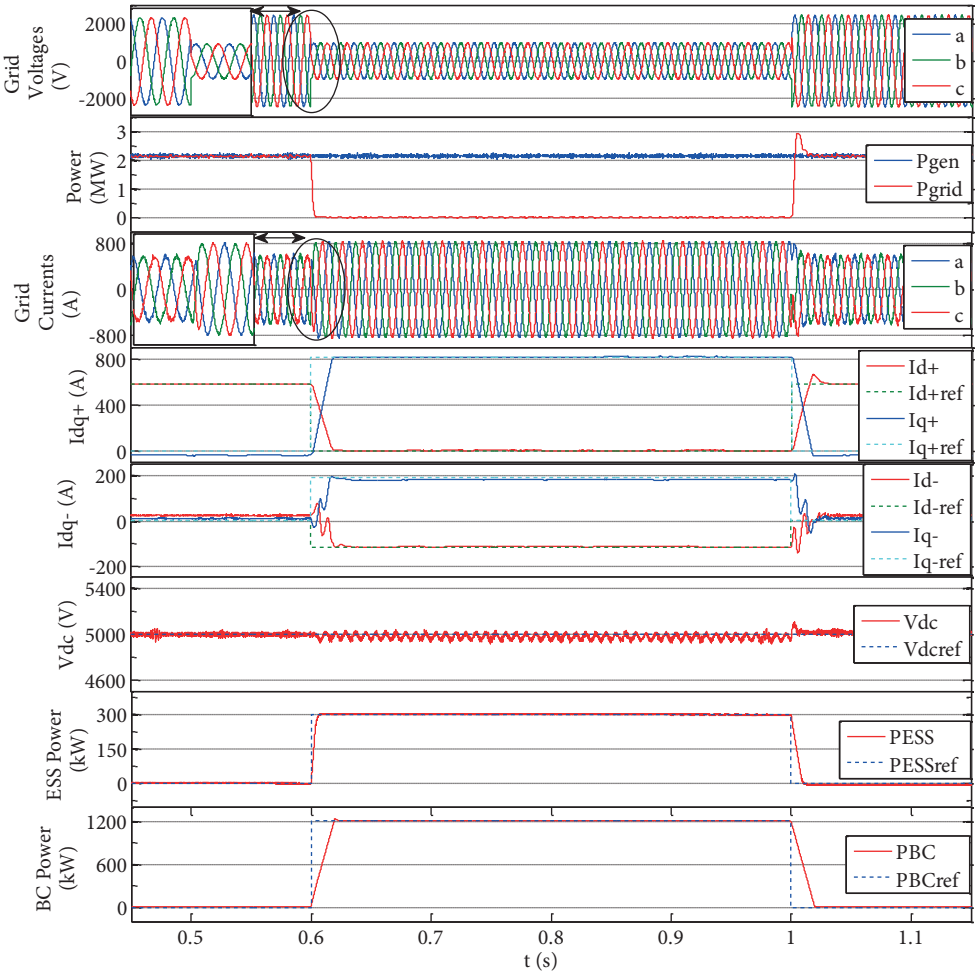

Figure 8. Simulation results for third scenario, from top to bottom: grid voltages, generator power and injected power to the grid, grid currents, positive sequence dq components of grid current, negative sequence dq components of grid current, DC-link voltage, ESS power, and BC power.

by the reduced size ESS and the BC, while controllers push the current components to their reference values accurately.

5. Conclusion

In this paper a novel cost-effective FRT strategy is proposed for PMSG-based WTs during grid faults. The unbalanced current reference signals are calculated by a clear analytical approach that provides the demanded reactive current by grid codes (when disturbed) without pulsating active power injection. The overall system, controlled by the proposed FRT strategy, offers the capability of riding through the fully interrupted grid voltage for WTs, satisfying GCRs thoroughly.

The main point of this strategy is that it does not care about fault type or dipping voltage profile, while, on the other hand, the calculated reference currents are careful about the current protection threshold and are completely in compliance with GCRs.

Reducing the ESS's power rating makes it cost effective and affordable without any drawbacks in its performance. The reduced-size ESS properly controls DC-link voltage during faults and lets the GSC inject the calculated currents. The ESS reduces the DC-link voltage oscillatory term to almost negligible. Three different scenarios including asymmetric and symmetric faulty grid conditions have been analytically presented and simulated to confirm the validity and effectiveness of the proposed FRT strategy.

References

[1] U.S. Dept of Energy. 20%Wind Energy by 2030 Increasing wind energy's contribution to U.S. Electricity Supply. Washington, DC, USA: 2008.

[2] Boidjemal Z, Talebi R, Djeriri Y, Yahdou A. A novel direct torque control using second order continuous sliding mode of a doubly fed induction generator for a wind energy conversion system. Turk J Elec Eng & Comp Sci 2017; 25: 965-975.

[3] Ardjoun SAEM, Abid M. Fuzzy sliding mode control applied to a doubly fed induction generator for wind turbines. Turk J Elec Eng & Comp Sci 2015; 23: 1673-1686.

[4] Mohammadi J, Afsharnia S, Vaez-Zadeh S. Improved fault ride through strategy for doubly fed induction generator based wind turbines under both symmetrical and asymmetrical grid faults. IET Renew Pow Gen 2016; 10: 1114-1122.

[5] Karakaya A, Karakas E. Process time and MPPT performance analysis of CF, LUT, and ANN control methods for a PMSG-based wind energy generation system. Turk J Elec Eng & Comp Sci 2016; 24: 3609-3620.

[6] Fakhari Moghaddam Arani M, Mohamed Y. A. I. Assessment and enhancement of a full-scale PMSG-based wind power generator performance under faults. IEEE T Energy Conv 2016; 2: 728-739.

[7] Polinder H, VanDer Pijl F, DeVilder GJ, Tavner PJ. Comparison of direct-drive and geared generator concepts for wind turbines. IEEE T Energy Conv 2006; 3: 725-733.

[8] Nasiri M, Mohammadi R. Peak current limitation for grid side inverter by limited active power in PMSG-based wind turbines during different grid faults. IEEE T Sustainable Energy 2017; 1: 3-12.

[9] Yassin HM, Hanafy HH, Hallouda MM. Enhancement low-voltage ride through capability of permanent magnet synchronous generator-based wind turbines using interval type-2 fuzzy control. IET Renew Power Gen 2016; 3: 339-348.

[10] Li Sh, An R. Minimum number of permanent-magnet synchronous generators for coordinated low-voltage ride-through of induction generators in hybrid wind farms. Turk J Elec Eng & Comp Sci 2016; 24: 4970-4983.

[11] Hansen AD, Michalke G. Multi-pole permanent magnet synchronous generator wind turbines' grid support capability in uninterrupted operation during grid faults. IET Renew Power Gen 2009; 3: 333-348.

[12] E.ON Netz GmbH. Grid Code: High and Extra High Voltage. Germany 2006.

[13] Ma K, Liserre M, Blaabjerg F. Operating and loading conditions of a three-level neutral-point-clamped wind power converter under various grid faults. IEEE T Ind App 2014; 1: 520-530.

[14] Goksu O, Teodorescu R, Bak CL, Iov F, Kjær PC. Impact of wind power plant reactive current injection during asymmetrical grid faults. IET Renew Power Gen 2013; 5: 484-492.

[15] Song HS, Nam K. Dual current control scheme for PWM converter under unbalanced input voltage conditions. IEEE T Ind App 1999; 5: 953-959.

[16] Anderson PM. Analysis of Faulted Power Systems. 1st ed. New York, NY, USA: IEEE Press, 1995.

[17] Miret J, Camacho A, Castilla M, de Vicuna LG, Matas J. Control scheme with voltage support capability for distributed generation inverters under voltage sags. IEEE T Pow Elec 2013; 11: 5252-5262.

[18] Shin D, Lee K, Lee J, Yoo DW, Kim HJ. Implementation of fault ride-through techniques of grid-connected inverter for distributed energy resources with adaptive low-pass notch PLL. IEEE T Pow Elec 2015; 5: 2859-2871.

[19] Alepuz S, Busquets-Monge S, Bordonau J, Martinez-Velasco JA, Silva CA, Pontt J, Rodriguez J. Control strategies based on symmetrical components for grid-connected converters under voltage dips. IEEE T Ind Elec 2009; 6: 2162-2173.

[20] Geng H, Yang G, Xu D, Wu B. Unified power control for PMSG-based WECS operating under different grid conditions. IEEE T Energy Conv 2011; 3: 822-830.

[21] Kim KH, Jeung YC, Lee DC, Kim HG. LVRT scheme of PMSG wind power systems based on feedback linearization. IEEE T Pow Elec 2012; 5: 2376-2384.

[22] Conroy JF, Watson R. Low-voltage ride-through of a full converter wind turbine with permanent magnet generator. IET Renew Pow Gen 2007; 3: 182-189.

[23] Nguyen TH, Lee DC. Advanced fault ride-through technique for PMSG wind turbine systems using line-side converter as STATCOM. IEEE T Ind Elec 2013; 7: 2842-2850.

[24] Sivasankar G, Suresh Kumar V. Supercapacitor energy storage based-UPQC to enhance ride-through capability of wind turbine generators. Turk J Elec Eng & Comp Sci 2015; 23: 1867-1881.

[25] Abbey C, Joos G. Supercapacitor energy storage for wind energy applications. IEEE T Ind App 2007; 3: 769-776.

[26] Nguyen TH, Lee DC, Song SH, Kim EH. Improvement of power quality for PMSG wind turbine systems. In: IEEE 2010 Energy Conversion Congress and Exposition; 12–16 Sept 2010; Atlanta, GA, USA. New York, NY, USA: IEEE. pp. 2763-2770.

[27] Abazari S, Farajzadeh S, Taghipour Boroujeni S. Enhanced control of a DFIG-based system by sliding-mode control method during network disturbances. Turk J Elec Eng & Comp Sci 2016; 24: 3198-3211.

[28] Karami MM, Itami A. Implementation of SVC based on grey theory and fuzzy logic to improve LVRT capability of wind distributed generations. Turk J Elec Eng & Comp Sci 2017; 25: 422-433.

[29] Shabestary MM, Mohamed YAI. An analytical method to obtain maximum allowable grid support by using grid-connected converters. IEEE T Sustainable Energy 2016; 4: 1558-1571.

[30] Calle-Prado A, Alepuz S, Bordonau J, Nicolas-Apruzzese J, Cortés P, Rodriguez J. Model predictive current control of grid-connected neutral-point-clamped converters to meet low-voltage ride-through requirements. IEEE T Ind Elec 2015; 3: 1503-1514.

[31] Junyent-Ferre A, Gomis-Bellmunt O, Green TC, Soto-Sanchez DE. Current control reference calculation issues for the operation of renewable source grid interface VSCs under unbalanced voltage sags. IEEE T Pow Elec 2011; 12: 3744-3753.

[32] Alepuz S, Busquets-Monge S, Bordonau J, Martinez-Velasco JA, Silva CA, Pontt J, Rodriguez J. Control strategies based on symmetrical components for grid-connected converters under voltage dips. IEEE T Ind Elec 2009; 6: 2162-2173.

[33] Moawwad A, El Moursi MS, Xiao W. A novel transient control strategy for VSC-HVDC connecting offshore wind power plant. IEEE T Sustainable Energy 2014; 4: 1056-1069.

[34] Rodriguez J, Cortes P. Predictive Control of Power Converters and Electrical Drives. 1st ed. Chichester, UK: IEEE Wiley, 2012.

[35] Yaramasu V, Wu B, Alepuz S, Kouro S. Predictive control for low-voltage ride-through enhancement of three-level-boost and NPC-converter-based PMSG wind turbine. IEEE T Ind Elec 2014; 12: 6832-6843.